AGU PUBLICATIONS

JGR

Journal of Geophysical Research: Oceans

RESEARCH ARTICLE

10.1002/2017JC013159

Key Points:
- Northwest Laptev Sea circulation investigated with moorings and high-resolution CTD transects
- Vilkitsky Strait and Trough are major pathway for Kara Sea freshwater
- Vilkitsky Trough is a conduit for polynya-formed dense water to Eurasian Basin

Correspondence to:
M. A. Janout,
Markus.Janout@awi.de

Citation:
Janout, M. A., J. Hölemann, L. Timokhov, O. Gutjahr, and G. Heinemann (2017), Circulation in the northwest Laptev Sea in the eastern Arctic Ocean: Crossroads between Siberian River water, Atlantic water and polynya-formed dense water, *J. Geophys. Res. Oceans*, *122*, 6630–6647, doi:10.1002/2017JC013159.

Received 6 JUN 2017
Accepted 18 JUL 2017
Accepted article online 22 JUL 2017
Published online 24 AUG 2017

Circulation in the northwest Laptev Sea in the eastern Arctic Ocean: Crossroads between Siberian River water, Atlantic water and polynya-formed dense water

Markus A. Janout[1], Jens Hölemann[1], Leonid Timokhov[2], Oliver Gutjahr[3], and Günther Heinemann[4]

[1]Alfred Wegener Institute Helmholtz Centre for Polar and Marine Research, Bremerhaven, Germany, [2]Arctic and Antarctic Research Institute, St. Petersburg, Russia, [3]Max Planck Institute for Meteorology, Hamburg, Germany, [4]Environmental Meteorology, University of Trier, Trier, Germany

Abstract This paper investigates new observations from the poorly understood region between the Kara and Laptev Seas in the Eastern Arctic Ocean. We discuss relevant circulation features including riverine freshwater, Atlantic-derived water, and polynya-formed dense water, emphasize Vilkitsky Strait (VS) as an important Kara Sea gateway, and analyze the role of the adjacent ~250 km-long submarine Vilkitsky Trough (VT) for the Arctic boundary current. Expeditions in 2013 and 2014 operated closely spaced hydrographic transects and 1 year-long oceanographic mooring near VT's southern slope, and found persistent annually averaged flow of 0.2 m s^{-1} toward the Nansen Basin. The flow is nearly barotropic from winter through early summer and becomes surface intensified with maximum velocities of 0.35 m s^{-1} from August to October. Thermal wind shear is maximal above the southern flank at ~30 m depth, in agreement with basinward flow above VT's southern slope. The subsurface features a steep front separating warm (–0.5°C) Atlantic-derived waters in central VT from cold (<–1.5°C) shelf waters, which episodically migrates across the trough indicated by current reversals and temperature fluctuations. Shelf-transformed waters dominate above VT's slope, measuring near-freezing temperatures throughout the water column at salinities of 34–35. These dense waters are vigorously advected toward the Eurasian Basin and characterize VT as a conduit for near-freezing waters that could potentially supply the Arctic Ocean's lower halocline, cool Atlantic water, and ventilate the deeper Arctic Ocean. Our observations from the northwest Laptev Sea highlight a topographically complex region with swift currents, several water masses, narrow fronts, polynyas, and topographically channeled storms.

1. Introduction

The region between the Kara Sea and the Laptev Sea features numerous islands and complex bathymetry (Figure 1) and is characterized by landfast ice [*Divine et al.*, 2004] and mobile pack ice often year round. The topography is dominated by the 200 m-deep, 60 km-wide Vilkitsky Strait (VS), which is known as a major export pathway from the northeast Kara Sea to the western Laptev Sea [*Berezkin and Ratmanov*, 1940; *Pavlov et al.*, 1996; *Volkov et al.*, 2002; *Harms and Karcher*, 1999, 2005; *Panteleev et al.*, 2007; *Janout et al.*, 2015, hereafter J15]. The annual mean volume transport across VS is 0.5–0.6 Sv (Sv = 10^6 m^3 s^{-1}) and includes a significant volume of Kara Sea freshwater from the Ob and Yenisey [*Harms and Karcher*, 1999; *Panteleev et al.*, 2007; J15], two of the largest rivers on earth with a mean combined annual runoff of ~1000 km^3 [*Dai and Trenberth*, 2002].

Arctic rivers provide a first order contribution to the Arctic Ocean freshwater budget [*Aagaard and Carmack*, 1989; *Serreze et al.*, 2006] and hence influence the Arctic Ocean circulation and its impact on climate [*Zhang and Steele*, 2007; *Spall*, 2013], and it is therefore important to understand the dominant river water pathways and dispersal processes. Arctic freshwater content varies on interannual and interdecadal timescales [*Rabe et al.*, 2014], and has been linked to large-scale Arctic climate indices [*Proshutinksy and Johnson*, 1997; *Morison et al.*, 2012]. However, specific freshwater pathways are still poorly understood. Recent model-based and observations-based studies have shown that Kara Sea freshwater exits through Vilkitsky Strait in a surface-intensified current (Vilkitsky Strait Current, VSC; J15). Based on a two-decade high-resolution model

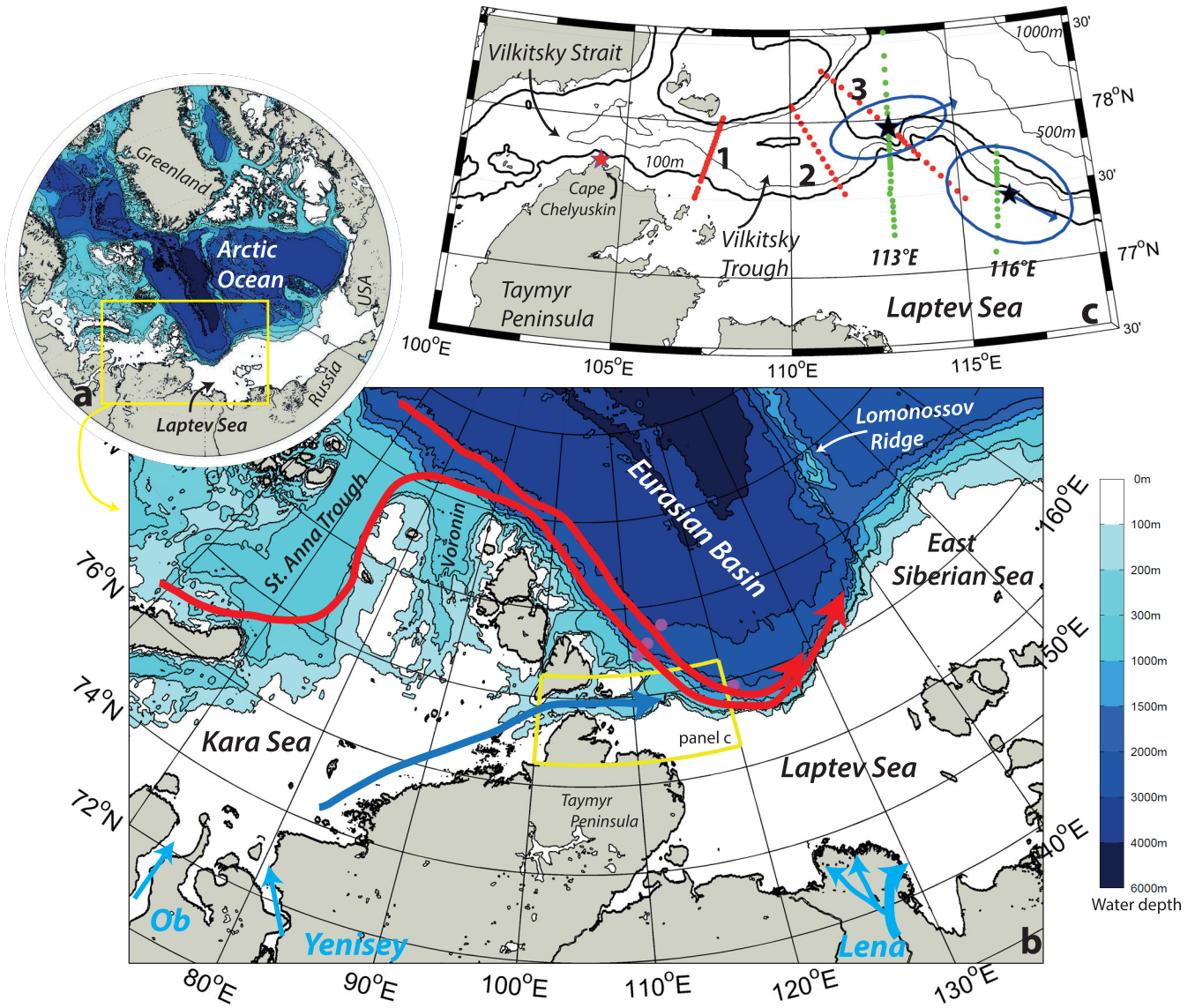

Figure 1. (a) Bathymetric map of the Arctic Ocean based on the International Bathymetric Chart of the Arctic Ocean (IBCAO) [*Jakobsson et al.*, 2008] and (b) a zoom into the Laptev Sea study region (note that the color scale is identical in Figures 1a and 1b). Arrows in blue and red indicate the location of the large Siberian Rivers (Ob, Yenisey, Lena) and sketch the pathways of the Kara Sea freshwater and the pathways of the Fram Strait and Barents Sea Atlantic water branches. The yellow box encircles the Vilkitsky Strait and Trough region enlarged in (c), which shows the location of weather station "Fedorova" at Cape Chelyuskin (red star), UCTD transects-1–3 in 2014 (red dots), the two 2013 transects (green dots), as well as the year-round oceanographic moorings (black stars) including the average ADCP-measured current direction at the mooring (arrows) and their variability ellipses.

run, the VSC varies seasonally and interannually and presumably follows the topographic slope between the Laptev Sea shelf and the adjacent submarine trough (Vilkitsky Trough, VT) and then propagates eastward along the Eurasian continental slope. It was suggested that a large part of the Eurasian freshwater input enters the Canada Basin [*Carmack et al.*, 2008; *Aksenov et al.*, 2011], where it is stored in the Beaufort Gyre [*Proshutinsky et al.*, 2009].

Submarine canyons and troughs are found around the Arctic continental slopes and are important topographic features that control the regional circulation [*Coachman and Barnes*, 1962; *Weingartner et al.*, 1998; *Itoh et al.*, 2015], enhance water mass transformation [*Hanzlick and Aagaard*, 1980; *Dmitrenko et al.*, 2014], feature upwelling [*Mountain et al.*, 1976; *Aagaard and Roach*, 1990; *Williams et al.*, 2006] and thus can present localized productive hotspots [*Grebmeier et al.*, 2015]. The ~250 km-long, 80 km-wide, and 200–350 m-deep VT is the easternmost of a series of large submarine glacial troughs in the northern Kara Sea adjacent to Voronin Trough and St. Anna Trough (SAT) [*Batchelor and Dowdeswell*, 2014]. In particular, SAT

plays an important role for the Atlantic water circulation in the Arctic Ocean, as it is a major pathway for the Barents Sea branch toward the Eurasian continental slope, where it meets the other major Atlantic water branch (i.e., Fram Strait branch) [*Rudels et al*., 1994]. Upon exiting SAT, both branches interact and subsequently cool during their eastward propagation along the Eurasian continental slope [*Rudels et al*., 1994; *Schauer et al*., 1997; *Pnyushkov et al*., 2015]. The regions north of Severnaya Zemlya (Figure 1) and the western Laptev Sea were hypothesized to be major dense water formation sites [*Martin and Cavalieri*, 1989; *Ivanov and Golovin*, 2007; *Bauer et al*., 2013], where cascading of near-freezing waters may provide one cooling mechanism for the Atlantic water boundary current [*Rudels et al*., 1994]. In addition, the neighboring VT is another large trough near the intersection between Atlantic water [*Rudels et al*., 2000; *Aksenov et al*., 2011] and river water pathways (J15), although its regional role for Atlantic water heat loss and mixing processes remains largely undiscussed as the area is only poorly studied.

In 2013 and 2014, the Russian-German "Laptev Sea System"-program concentrated enhanced efforts on the northwest Laptev Sea in order to learn more about regional circulation and associated freshwater pathways. Two summer expeditions carried out several detailed hydrographic transects and deployed and recovered 1 year-long oceanographic mooring in VT. The aim of this paper is to shed more light on processes and circulation features in and around VT, with an emphasis on riverine freshwater pathways, Atlantic water circulation, and dense water formation.

2. Data and Methods

2.1. Hydrographic Transects and Mooring

VT measurements were carried out during *Transdrift* 21 (4–17 September 2013) and *Transdrift* 22 (13–28 September 2014) to the Laptev Sea aboard *RV Viktor Buinitsky*. Multiple cross-trough transects were completed using an *Ocean Science* Underway (U)CTD system complemented by full water sampling stations using a *Seabird 19plusV2 (Seacat)*-profiler. The UCTD uses *Seabird* sensors providing accuracies of the processed data of 0.004°C and 0.002–0.005 S m^{-1} for temperature and conductivity at a sampling rate of 16 Hz. The *Seacat* sampled with 4 Hz with initial accuracies of 0.005°C and 0.0005 S m^{-1} for temperature and conductivity, respectively. Data are stored internally on the UCTD probe and downloaded subsequently via Bluetooth connection. The profiling time determines the measurement depth and is estimated before each cast based on presumed water depth and ship velocity. However, considering sometimes inaccurate bathymetric charts and rapidly changing topography in this region, not every CTD cast reached to the near-bottom, in particular above the slopes as seen in the data gaps in transect-3 in 2014 (Figure 2). The horizontal distance between UCTD casts varied during the surveys and depended on ship velocity, water depth, and the scientific decision to sample with high lateral resolution.

One oceanographic mooring deployed at the southern base of VT at a depth of 320 m (77.95°N, 113.0°E, Figure 1) operated from 4 September 2013 to 14 September 2014 and was equipped with CTDs and two *TRDI Workhorse Sentinel* ADCPs (Acoustic Doppler Current Profiler; one upward-looking 300 kHz moored 30 m below surface and one downward-looking 150 kHz instrument moored at 40 m depth). The vertical current coverage is unfortunately limited to the upper 200 m due to erroneous measurements below that depth. The ADCPs recorded hourly ensembles using 1 m (300 kHz) and 4 m (150 kHz) bins. The 300 kHz ADCP's compass headings from the sea ice drift is in good agreement with satellite sea ice drift (see section 2.3), which gives us good confidence regarding the quality of upper ocean current directions [*Janout et al*., 2013]. The principle current components from the nearest bins between the two ADCPs are in near-perfect agreement except that they are offset by 55°, which we assume constitutes an offset in the 150 kHz ADCP's compass. This however has no implications for our results. Seven *Seabird SBE37* resolved the temperature and salinity of the water column below 30 m with half-hourly sample intervals providing accuracies of 0.002°C and 0.0003 S m^{-1}. In addition, two *RBR* and one *Sea and Sun* optical backscatter recorder provided turbidity measurements. Further, vertically averaged current velocities and direction were extracted from a mooring located at the 80 m-isobath (77.5°N, 116.5°E) that recorded currents and hydrographic parameters from September 2014 to September 2015.

2.2. Atmospheric Information

Wind speed and direction-records were received from weather station "Fedorova" (WMO station 20292) located at 77.72°N, 104.3°E at Cape Celjuskin in Vilkitsky Strait (Figure 1). The station provides hourly

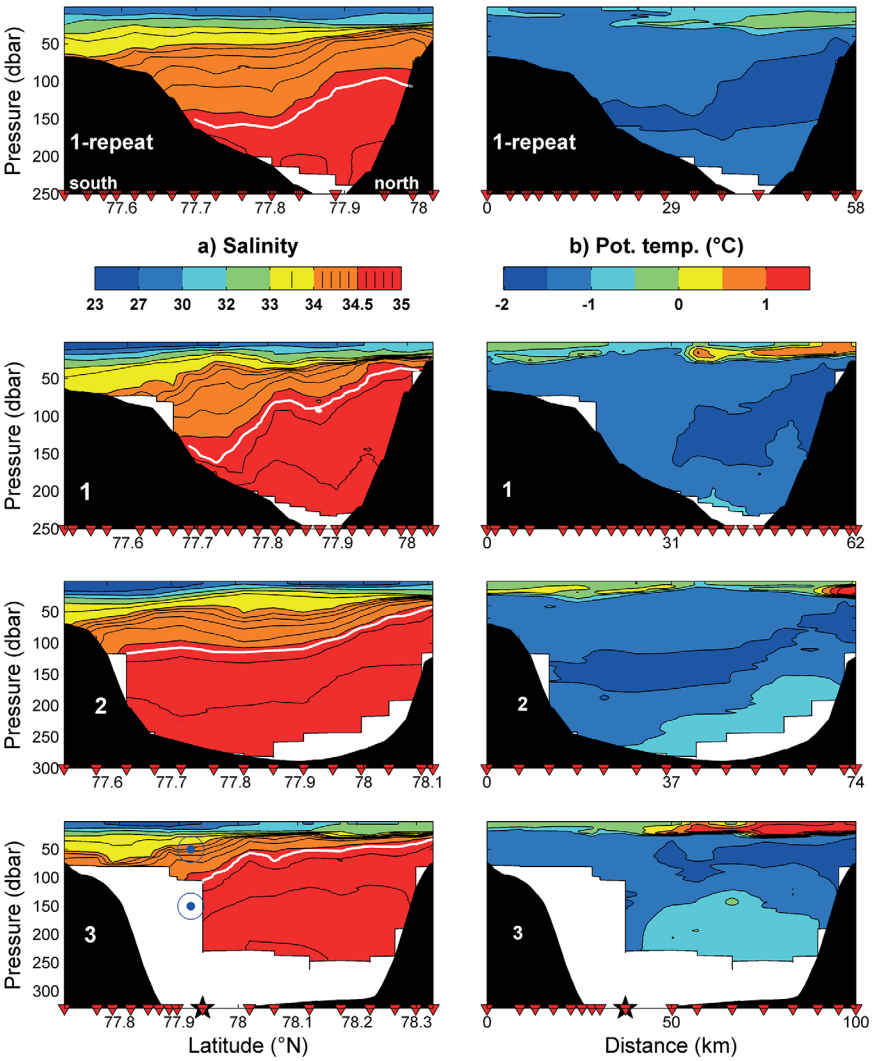

Figure 2. UCTD (a) salinity and (b) potential temperature transects across Vilkitsky Trough on 13–15 September (transects-1–3) and 27 September 2014 (transect-1-repeat). The station locations are indicated by the red triangles at the bottom. The along-track position is provided (left) in latitude (°N) as well as (right) in distance (km). The cross-trough bathymetry was extracted from IBCAO [*Jakobsson et al*., 2008]. Note the nonlinear color scale for salinity, increments of 0.1 are provided with black contours for salinity >34.0. The black star shows the mooring location in transect-3 (see Figure 1 for location). The currents are on average directed out of the page (i.e., down-trough) at the mooring location, sketched in the figure by the dot in a circle. The white contour $\sigma_\theta = 27.8$ kg m^{-3} is shown to indicate that the density structure is controlled by the isohalines.

information on pressure, temperature, and winds, and has been in operation since 1933 (with interruptions in the 1940s). We further used wind data from the global reanalysis data (~80 km horizontal resolution) set ERA-Interim (ERA-I) [*Dee et al*., 2011]. Furthermore, we employed results from two simulations with the non-hydrostatic regional climate model COSMO-CLM [*Rockel et al*., 2008] performed for the period November 2013 to April 2014. COSMO-CLM was double-nested within ERA-I at horizontal resolutions of 15 km followed by 5 km. COSMO-CLM utilizes sea ice concentration that was prescribed daily from the AMSR2-satellite product [*Wentz et al*., 2014], and sea ice thickness initialized with the PIOMAS reanalysis data set [*Zhang and Rothrock*, 2003]. For more detailed information on COSMO-CLM, please refer to *Gutjahr et al*. [2016].

2.3. Sea Ice Drift and Concentration

Sea ice drift was provided by the European Space Agency (ESA) via the Center for Satellite Exploitation and Research (CERSAT) at the *Institut francais de recherche pour l'exploitation de la mer* (Ifremer), France, and was used in this paper to verify the ADCPs compass direction by comparing local ice drift with larger-scale satellite-derived ice drift. The motion fields are available from September until May since 1992 and are based on

a combination of drift vectors estimated from scatterometer and radiometer data. The data are provided at a grid size of 62.5 km, using time lags of 3 days. Details on data processing and validation are provided by *Girard-Ardhuin and Ezraty* [2012], and the accuracy of these drift estimates was additionally discussed by *Krumpen et al*. [2013]. Sea ice presence and drift above the mooring were estimated from the ADCP's bottom track by use of a threshold of the error velocity, which rapidly increases once sea ice disappears as a solid reflector [*Belliveau et al*., 1990].

3. Results

3.1. Water Masses in Vilkitsky Trough

VT's hydrographic structure was investigated with a series of detailed UCTD transects in September 2014 (Figure 2) complemented by two transects sampled in 2013 (Figure 3). In 2014, surface waters were the freshest (23–27) on the south side above the shelf-trough slope (Figure 2), largely in agreement with the modeled position of the Vilkitsky Strait Current (VSC, J15), which transports low-salinity waters from the Kara Sea to the western Laptev Sea. These low-salinity waters contrast with the more saline (30–32) surface waters above the trough's northern flank. All surface (0–20 m) waters were well above freezing, with temperatures of ~0°C in the dilute waters presumably of coastal Kara Sea origin above the southern slope, and maximum temperatures (>2°C) in the northern half of the trough in all transects (Figure 4). The warm waters in this low-salinity range are likely remnants of summer-surface warming during ~2 months of open water in much of the Kara Sea prior the expedition. Besides a small area of ice that was stuck in between islands northwest of VS, the greater region was ice free during both 2013 and 2014 September surveys until freezeup occurred in early October.

The deeper (>100 m) parts of VT are filled with saline (>34.5) waters, with proportionally larger volumes toward the trough's mouth. Temperatures in most of the interior trough were −1.5 to −1.0°C, while the coldest waters (<−1.5°C) occupied the northern slope at 40–200 m depth with salinities between 34.6 and 34.7 (Figure 2). Equally cold waters were found in September 2013, except that they extended from the Laptev Sea shelf down the slope and into VT (Figure 3). These cold and saline waters are likely products of winter freezing processes in polynyas over adjacent shelf regions [*Timokhov et al*., 2015; *Preußer et al*., 2016], which indicates that VT is a pathway for shelf-cooled waters toward the Nansen Basin. The cold waters overlaid warmer (−1.0 to −0.5°C) and saline (>34.7) Atlantic-derived waters that enter the Arctic Ocean from the Barents Sea via St. Anna Trough and follow the topography into VT along its northern flank [*Aksenov et al*.,

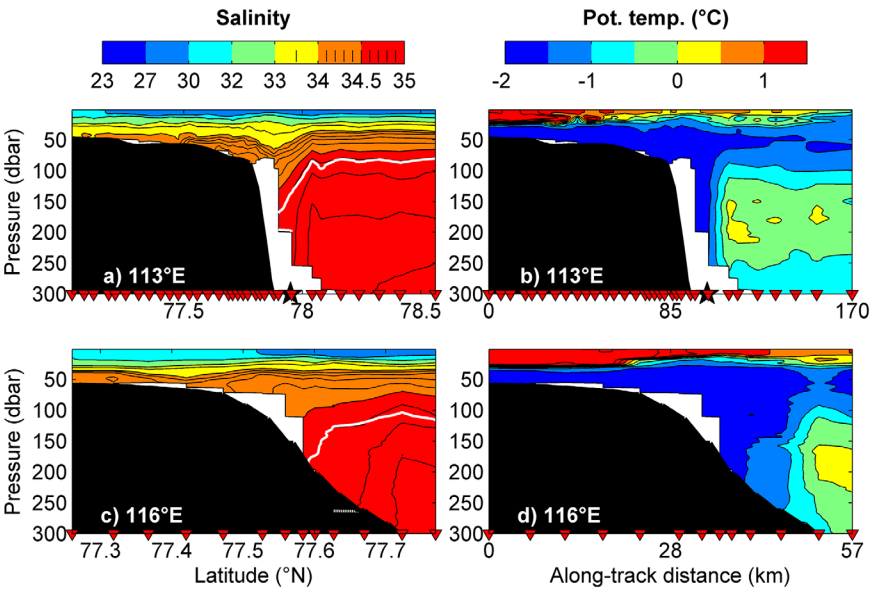

Figure 3. Same as Figure 2, except for transects (top) 113°E and (bottom) 116°E sampled in September 2013. Please note that a similar figure was previously published in J15.

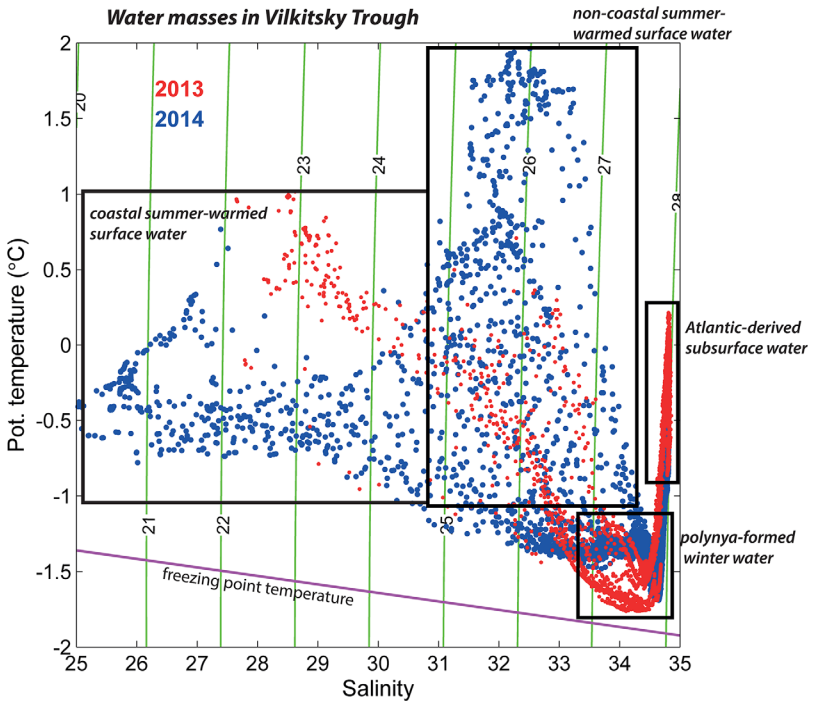

Figure 4. Temperature-salinity diagram including the freezing point temperature (magenta line) and sigma-contours (green lines) showing the relevant water masses that are present in Vilkitsky Trough in 2013 (red dots) and 2014 (blue dots).

2011]. This is supported by a September 2013 CTD profile collected by the *Nansen and Amundsen Basins Observational System* (NABOS) about 300 km upstream above the continental slope north of Severnaya Zemlya, which had the same hydrographic properties as those measured in VT during the same time (not shown). This water mass was largest in volume at the mouth (transect-3), decreased and sloped up the northern edge of the trough in transect-2, and showed only a trace near the bottom of transect-1 (Figure 2). Similar waters were found in September 2013 across the mouth of VT, with core temperatures as warm as +0.5°C (Figure 3).

The salinity (and density) distribution in our cross-trough transects is consistent with J15's suggested propagation of a dilute surface-intensified current above the southern slope. Thermal wind shear estimated from the cross-trough density structure provides rough insights on baroclinic geostrophic currents. However, the region is topographically complex and impacted by tides, and we further lack the ancillary information necessary to convert thermal wind shear into absolute geostrophic velocities. Nevertheless, consistent with tilted isohalines (and isopycnals) toward the southern slope (Figure 2), we find maximum thermal wind shear (referenced to the surface, not shown) at ~30 m depth. This implies a baroclinic geostrophic surface-intensified down-trough flow, consistent with generally eastward flow as suggested by modeling studies and our mooring near VT's confluence. For more reliable transport estimates across VT, it would be desirable to operate shipboard along-track velocity measurements in future surveys, which was unfortunately not an option during the 2013 and 2014 expeditions.

3.2. The Short-Term Effect of Blocking-Favorable Winds

The recent model studies by J15 presented monthly means and showed a primarily stable VSC that varies on seasonal and interannual time scales but did not provide any insights regarding shorter-term variability. Our 2014 campaign allowed a repeat of transect-1 after 2 weeks (Figure 2), and strikingly found that the low-salinity core was absent and isohalines leveled out compared with the first visit. To better illustrate these changes, we estimate the thickness of a freshwater layer H_{FW} present in the upper 50 m of the water column across each of the three transects (Figure 5), assuming a reference salinity of $S_{ref} = 34.80$ following *Aagaard and Carmack* [1989]:

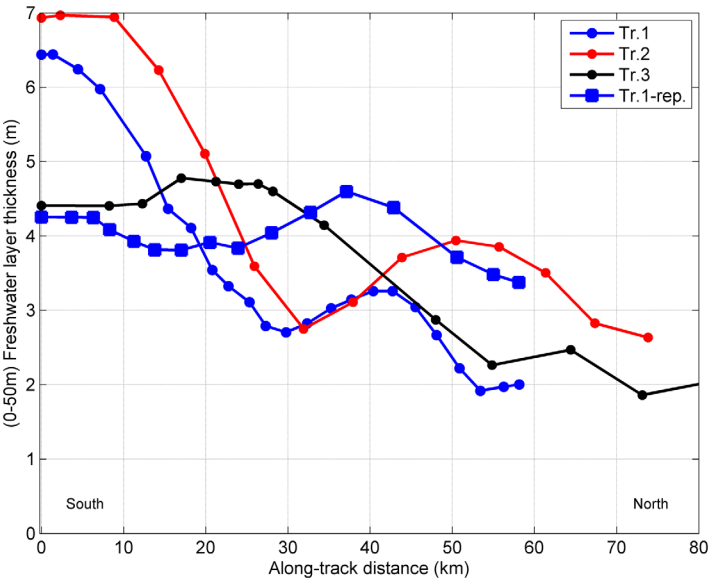

Figure 5. Integrated 0–50 m freshwater layer thickness H_{FW} (m) along each of the four 2014 cross-trough transects (Figure 2, and Figure 1 for location map) versus along-track distance (km).

$$H_{FW} = \int_0^{50m} \frac{S_{ref} - S}{S_{ref}} dz \quad (1)$$

Further, down-trough freshwater transport F_{FW} is computed by integrating the product of down-trough velocities and the freshwater content over the width and vertical extent of the low-salinity core:

$$F_{FW} = \int_0^{50m} \int_0^{20km} u \times \frac{S_{ref} - S}{S_{ref}} dzdx \quad (2)$$

The first visit shows an integrated freshwater content of H_{FW} >6 m on the south side, and >2 m on the north side of transect-1 (Figure 5), while the repeat transect shows a nearly evenly distributed H_{FW} of ~4 m across the width of the trough. The total mean H_{FW} content along transect-1 only slightly increased from 3.6 to 4.0 m, which implies that freshwater was not removed but mainly redistributed. This can be explained by strong easterly winds above VT into Vilkitsky Strait due to low pressure over the southwestern Laptev Sea (not shown). These winds were oriented against the generally eastward flow and led to blocking of the VS outflow and to northward surface Ekman transport, which apparently spread the fresh waters from the southern flank across VT coincident with a southward spreading of the cold waters at 150–200 m (Figure 2). Blocking-winds such as these were found to dominate the variability in VS transport [*Harms and Karcher*, 2005; J15] on interannual time scales but can also cause higher frequency variability in the region's currents and water mass structure. While the salinity cross-strait structure changed significantly over 2 weeks, the thermal structure remained largely intact, except with a reduction in upper layer temperatures (Figure 2). This is expected as late September is a transition season there, where air temperatures remain generally constant below freezing. The temperature change (ΔT) of a water layer due to air-sea fluxes is calculated with $\Delta T = (HF_{net}t)/(\rho_w c_w H)$. Assuming a mean ERA-I net heat flux of $HF_{net} = 36$ W m^{-2} over $t = 14$ days, $\rho_w = 1025$ kg m^{-3}, $c_w = 4.26$ kJ kg^{-1} K^{-1} amounts to a cooling of a $H = 20$ m-thick surface layer by 0.5 K. The average cross-strait temperature reduction in the upper 20 m was 0.6 K, which hence is explained by surface fluxes rather than by internal ocean dynamics.

3.3. 2013–2014 Mooring Observations in Vilkitsky Trough

3.3.1. Hydrographic Variability

One oceanographic mooring was placed at the 320 m-deep base of VT, near the front between the warm Atlantic-derived waters in the central trough and the cold waters above the slope (Figures 2 and 3). The hydrographic structures during the 2013-deployment and 2014-recovery were nearly similar, with strong stratification in the upper 30 m and surface salinities of 29 in 2013 and <26 in 2014 (Figure 6). Surface waters were slightly warmer in 2013 and also influenced by warmer (>−1.0°C) water below 200 m, which dominates the year-long temperature record at this location except during late winter and spring (Figure 7). Temperatures episodically increased to a maximum of 0°C at depths below ~150 m, most frequently in the first half of the record, which is likely due to temporary displacements of the front. After March 2014, warm periods were sparse and the water column primarily cold. The low-pass filtered temperature recorded by the uppermost instrument at 30 m did not get above −1.4°C, and was below −1.8°C from November until May (Figure 8). Salinity indicated year-round stratification between 30 and 70 m (Figure 7), except in February–March following a period of steadily increasing near-surface salinity since late November from 33.4 to 34.1 (Figure 8) likely as a consequence of ice formation and salt rejection. Based on the ADCP's bottom track velocities, the mooring was covered by mobile pack ice from November 2013 until late May 2014 (Figure 7).

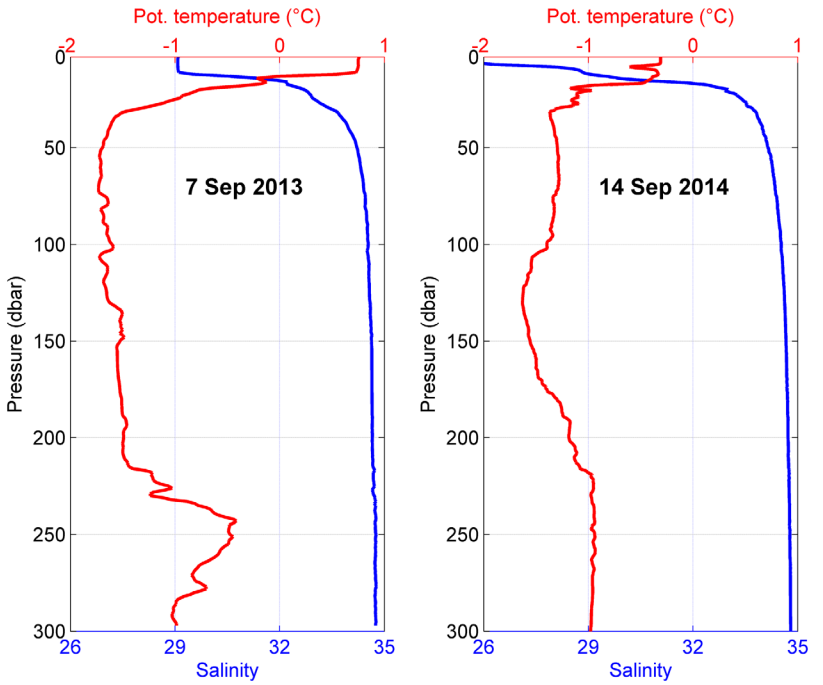

Figure 6. Potential temperature (°C, red) and salinity (blue) profiles at the Vilkitsky Trough mooring location during mooring deployment (7 September 2013) and recovery (14 September 2014).

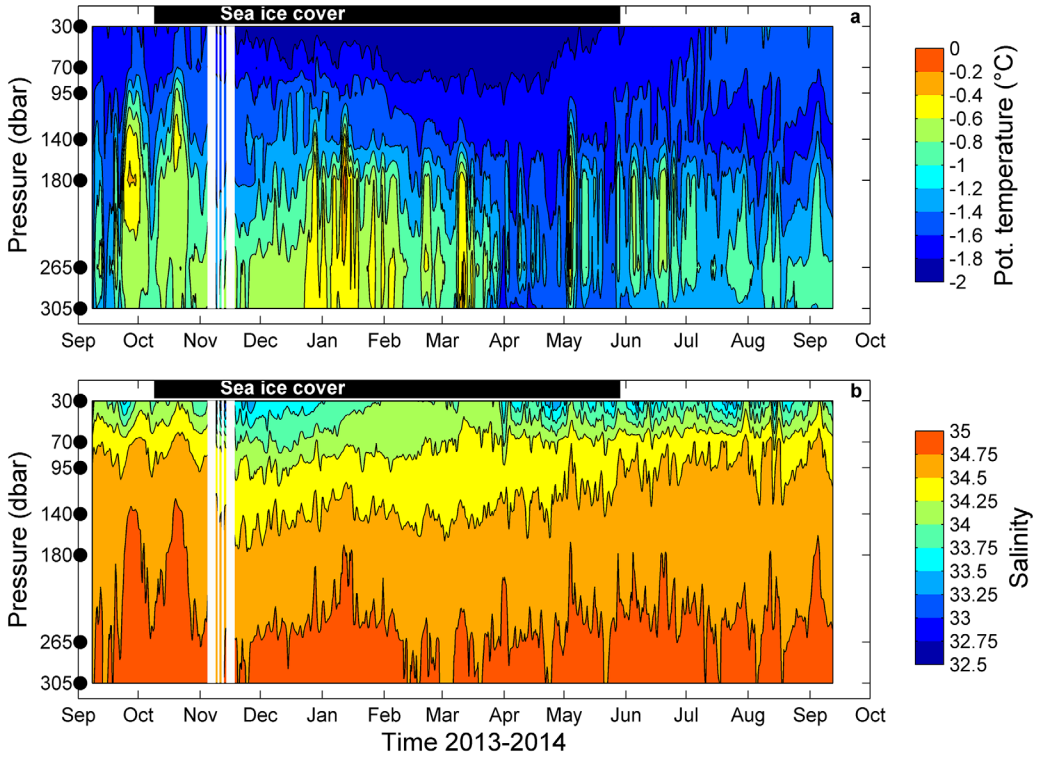

Figure 7. (a) Potential temperature (°C) and (b) salinity time series of the Vilkitsky mooring versus pressure (dbar) from September 2013 to September 2014. The contoured plots are composed from seven CTDs mounted at depths that are indicated as dots and depth labels on the *y* axis. The black bar at the top indicates when sea ice was present based on the ADCP bottom track record. Please note the blanking of some periods in November 2013, when a storm event caused considerable subduction of the instruments (see section 3.3.3).

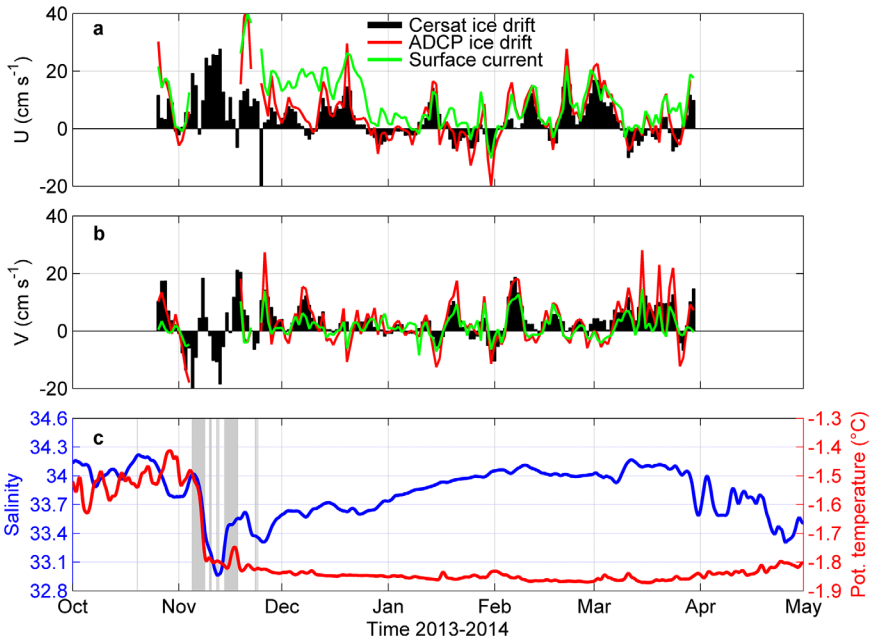

Figure 8. (a) Zonal and (b) meridional components of daily mean CERSAT-ice drift (black), ice drift from the ADCP bottom track (red), and near-surface currents (green, all in cm s^{-1}). The CERSAT ice drift product is used to verify the compass direction of the upper ADCP and is most reliable before April and hence not shown after that; (c) 24 h low-passed 30 m-temperature (°C, red) and salinity (blue) record. The grey bars indicate times when the mooring was subducted and where values were removed and interpolated. Note that ADCP recordings during this time in Figures 8a and 8b are faulty and are hence removed.

Sea ice is commonly landfast in VS and along the Laptev Sea coast [*Bareiss and Görgen*, 2005], although several winters within the last decade featured thin and mobile ice in and even west of VS [*Preußer et al.*, 2016].

3.3.2. Currents

The largest part of the current and ice drift variability is concentrated in the semidiurnal frequency band. Semidiurnal tides, in particular at the M_2-frequency are clockwise polarized at this location as is the case on the Laptev Sea shelf [*Janout and Lenn*, 2014], although semidiurnal oscillations are often masked by the swift down-trough currents that dominate this location. Semidiurnal oscillations are clearest in the near-bottom pressure record (not shown), and dominated by the M_2, S_2, and N_2-frequencies based on harmonic analysis using the Matlab T-Tide package [*Pawlowicz et al.*, 2002] (Table 1).

The currents measured by ADCPs at the mooring location adjacent to the southern slope of VT are on average oriented eastward (down-trough), and exhibit a seasonal cycle as highlighted by monthly mean current velocities (Figure 9). From September through December, the velocities were highest (20–25 cm s^{-1}) in the upper 70–100 m, and subsequently decreased to still comparatively swift down-trough, flow of 15–20 cm s^{-1}. Below that the flow decreased to a minimum nearly vertically homogenous flow of 10–15 cm s^{-1}. August and September 2014 currents were surface intensified (25–30 cm s^{-1}). The velocities at this location were seasonally enhanced into early winter when sea ice was already present, and roughly agree with J15's modeling results which showed the largest velocities in Vilkitsky Strait during fall and minimum flow in April–June consistent with the mooring-recorded monthly mean velocities. The annually averaged flow is 20 cm s^{-1} and persistently oriented down-trough, which implies that VT is a steady topographic pathway for water masses both in the surface and below that are either exported from the Kara Sea or that are formed locally on the adjacent shelves and slopes. The currents and in particular the ice drift velocities nevertheless varied considerably on time scales anywhere between a few days to weeks, often related to the passage of storms through

Table 1. Tide Parameters Including Standard Deviations (in Parentheses) Computed From a 15 m-Above-Bottom Pressure Record

Tidal Constituent	Amplitude (m)	Phase	SNR
M2	0.17 (0.005)	85 (2)	1000
S2	0.08 (0.005)	161 (4)	240
N2	0.03 (0.005)	43 (12)	27
O1	0.03 (0.007)	238 (13)	17
K1	0.05 (0.006)	278 (8)	58

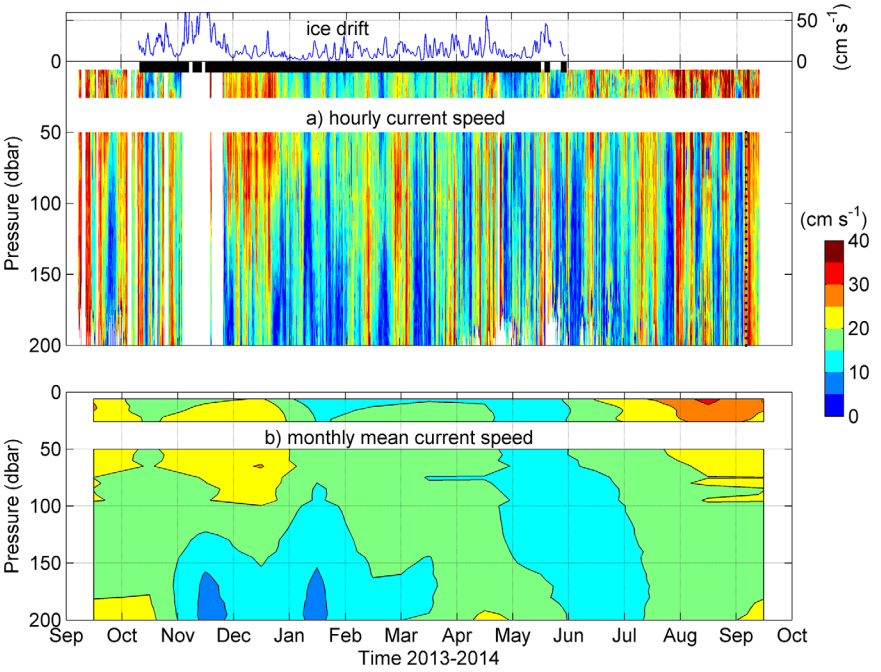

Figure 9. (a) Hourly and (b) monthly averaged current speed from September 2013 until September 2014 versus depth (m) from the mooring at the mouth of Vilkitsky Trough. Periods of faulty data due to mooring subduction in November 2013 were left blank in Figure 9a and not used to compute the November mean in Figure 9b. The black bar indicates the presence of sea ice at the location, overlaid by sea ice drift (cm s^{-1}) from the ADCP's bottom tracking function.

the region. These flow field variations coincide with hydrographic variability and will be subject of further discussion below.

3.3.3. On Topographic Winds in Vilkitsky Strait and Freezeup in November 2013

In mid-November, the topmost (30 m) CTD-record showed an abrupt decrease in both salinity (from >34 to 33.4) and temperature (from −1.4 to −1.8°C) over the course of a few days (Figure 8). This event was triggered by strong westerly winds parallel to the northeast Kara Sea coast into VS due to a low pressure system centered over Svalbard (Figure 10). During this time, the mooring was temporarily subducted by more than 100 m based on the upper *SBE37*-pressure record, and satellite derived as well as locally measured ice drift and currents were strongly elevated (Figure 8), consistent with an intensified (wind-driven) Kara Sea outflow. The temperature and salinity of the upper layer changed abruptly during the storm, manifested by a steep 30 m-salinity decrease following vertical mixing of low-salinity near-surface waters, and a temperature decrease due to intense ocean heat loss during the storm.

The November 2013 event marked the final transition into winter. Freezeup already began in mid-October as indicated by satellite images and the mooring's bottom track, although the upper layer (0–30 m) cooling to near-freezing was delayed until this November storm. This storm period included maximum wind speeds of >25 m s^{-1} measured at a weather station in Vilkitsky Strait and affected the area like no other storm during the year-long record, although extreme wind speeds around the mooring location are neither shown in ERA-I nor NCEP [*Kalnay et al*., 1996] winds. The discrepancy may be related to insufficient resolution of the reanalysis grids in the geographically complex region between the Kara and Laptev Seas as underlined by a comparison between ERA-I (80 km resolution) and a 5 km (C05) and 15 km (C15) resolution atmospheric model. During this storm, wind speeds in the northeast Kara Sea exceeded 20 m s^{-1} in all three wind products. However, east of VS ERA-I winds were only moderate (<14 m s^{-1}), while high-velocity winds extended all the way past the mooring location in C15 and C05. A 2 week average from 4 to 17 November 2013 highlights ~30% stronger winds and more intense ocean heat loss by 20–220 W m^{-2} in C05 than in ERA-I due to channeling through VS and other gaps between islands, as well as close to the Taymyr coast (Figure 10). This occurred on scales too small to be resolved by global reanalysis products, which implies that coarsely resolved models underestimate ocean circulation and heat fluxes during storm events and hence underlines the need for high-resolution studies in dynamic areas such as the northwest Laptev Sea. Similar

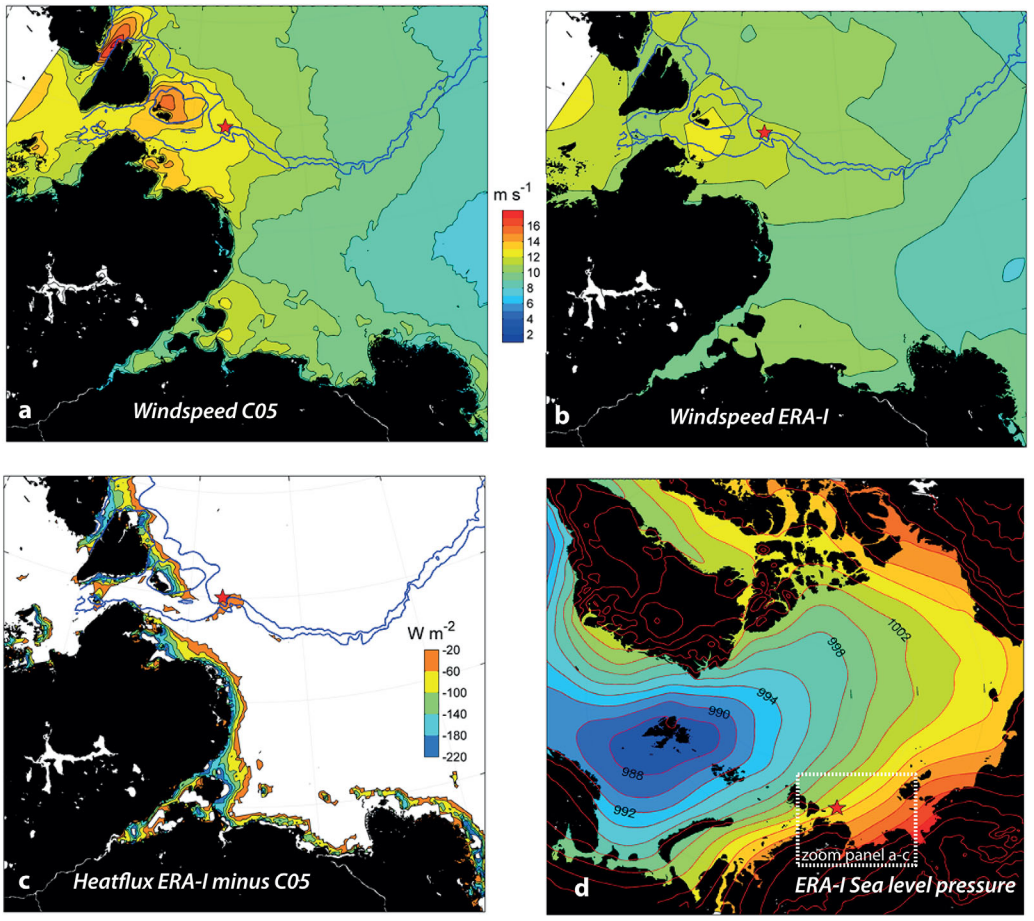

Figure 10. Mean 4–17 November 2013 maximum 10 m wind speed (m s^{-1}) from (a) COSMO-CLM with 5 km resolution (C05) and (b) ERA-I; the red star marks the mooring location. (c) Heat flux difference (W m^{-2}) between ERA-I and C05 during this 2 week period. Blue contours mark the 100 and 300 m-isobaths. (d) Mean sea level pressure (mbar) over the Arctic Ocean during this 2 week period.

conclusions were reached for other high-latitude regions, such as around Greenland [*Moore et al.*, 2015] and Novaya Zemlya [*Moore*, 2013].

4. Discussion

The Vilkitsky Strait and Trough region is an important crossroads between several different circulation features that are all releveant for the eastern Arctic Ocean. The observations presented above will next be discussed with a particular focus on three subjects: (a) Kara Sea freshwater pathways, (b) the circulation of Atlantic water and possible implications for the Laptev Sea shelf, and (c) dense water formation and associated pathways.

4.1. Kara Sea Freshwater Pathways

Moored current observations and considerable thermal wind shear above the southern trough's slope at 20–30 m computed from the UCTD hydrographic transects largely confirm the model observations presented in J15, with a generally eastward surface-intensified current that carries dilute Kara Sea water toward the Nansen Basin along the Laptev Sea continental slope. The amount of freshwater H_{FW} present above the southern slope decreases slightly from ~7 to ~5 m between VS (transect-1) and the mouth of VT (transect-3; Figure 5), which implies a relatively steady along-slope freshwater transport, as further supported by steady eastward upper layer velocities measured by the ADCP. Considering mean 0–50 m H_{FW} of 4.5 m at transect-3 (Figure 5) and mean September currents of 25 cm s^{-1} (Figure 9) over the same depth across a presumed current width of ~20 km (J15) suggests a September mean freshwater transport of 23 mSv. This is equivalent to 58 km^3 of freshwater in September and agrees well with mean modeled September

estimates (J15). Overall, our CTD surveys generally support the assumption that much of the Kara Sea freshwater remains within the VSC, although strong winds are clearly able to disrupt the mean flow and divert freshwater onto the shelf. Further observations-based VSC pathways are difficult to map due to the lack of concurrent moorings. Although not overlapping temporally, one additional mooring ~100 km east of the VT-mooring (Figure 1) recorded currents near the shelf break at the 80 m-isobath from September 2014 to 2015. There the vertically averaged annual mean flow was 8 cm s^{-1} along the southeastward principal current axis (139°T), which is aligned with the sloping bathymetry and lends further support for the modeled eastward pathway of the VSC. In combination, UCTD transects (Figures 2 and 3) and moorings indicate persistent eastward topographically guided flow that carries freshwater eastward along the continental slope. The confluence of VT with the continental slope hence introduces distinct biogeochemical signatures to this region, as was found by stable isotopes-based water mass classifications [*Bauch et al*., 2016], as well as by biomarkers studies [*Kaiser et al*., 2017]. Nevertheless, quantifying freshwater dispersal and exact pathways requires detailed synchronized mooring programs with the challenging task to measure salinity near the surface.

4.2. Atlantic Water Variability in Vilkitsky Trough

The presence of warm Atlantic water at the Eurasian continental slope at depths below ~200 m previously raised questions about whether upwelling of these warm waters may occur on the Siberian shelves [*Dmitrenko et al*., 2010], similar to observations along the Beaufort shelf in the western Arctic [*Pickart et al*., 2009]. The complex topography of the northwestern Laptev Sea presents itself as a potential candidate where such upwelling could occur. Our oceanographic mooring was placed near a strong front between cold, less saline shelf waters and the warmer Atlantic-derived waters in central VT, and measured a swift mean along-trough flow of ~20 cm s^{-1} toward the Nansen Basin. The subsurface currents at the mooring are quite persistent but show episodic deviations, which coincide with departures in temperature and salinity indicating frontal movement. The largest variability in the year-round records is seen at 180 m with temperatures between −1.5 and +0.5°C (Figure 7). An analysis of squared-coherency between the 180 m-temperature record and 150 m-currents showed statistically significant peaks at semidiurnal as well as at 1.5–2 day periods, which suggests that the local wind field does not entirely explain the frontal variability. A detailed look into these time series shows that the hydrographic front is mostly located north of the VT-mooring, so that low temperatures, lower near-surface salinity and swift down-trough flow prevail until the flow field is disrupted and temperatures increase episodically. These reversals are not always observed throughout the water column but are sometimes limited to the subsurface and not necessarily coincident with sudden wind changes, which points to upstream effects such as propagating shelf edge waves as was discussed for canyon upwelling processes in the western Arctic [*Pickart et al*., 2009]. Episodic temperature increases of >1 K generally occur for a few days, and only once lasted as long as 1 week in early May 2014 (Figure 11), when the flow reversed from 30 cm s^{-1} down-trough to 12 cm s^{-1} up-trough (Figure 12). Progressive vector calculations based on the measured velocities at the mooring suggest a maximum theoretical frontal displacement during early May of 30 km toward the trough's southern edge, but less (<10 km) during shorter events. This suggests that these events are mainly short lived and we have no indications that the warm Atlantic-derived waters from below 150 m are transferred onto the shelf. In contrast to that, the hydrographic structure in VT could allow for along-isopycnal on-shelf transport (Figures 2 and 3). Near-surface densities in VT are similar to near-bottom densities on the northwest Laptev Sea shelf, which suggests that the more saline and summer-warmed near-surface waters in VT outside the freshwater core could propagate along isopycnals onto the shelf to depths of ~50–80 m. One such large event might have occurred in summer 2009, when waters with characteristics similar to those measured over VT (S ~ 34, T ~ −1.0°C) occupied the bottom waters throughout most of the shelf for nearly 1 year [*Janout et al*., 2013]. These properties were first observed in the northwest Laptev Sea, then spread eastward across the shelf and persisted until winter processes reset the hydrography.

The extended open water seasons on Arctic shelves in recent years significantly increases the role of solar warming for the oceanic heat budget [*Perovich et al*., 2008], although vertical Atlantic water heat transport processes are not sufficiently understood in that region and still need further investigations. So far Atlantic water properties as commonly found below 150–200 m north of the Laptev Sea continental slope or in VT (Figure 3) were not yet found on the shelf. This either implies that stratification and fronts are too strong in the region to allow for significant upwelling or that upwelling occurs only localized and episodically and

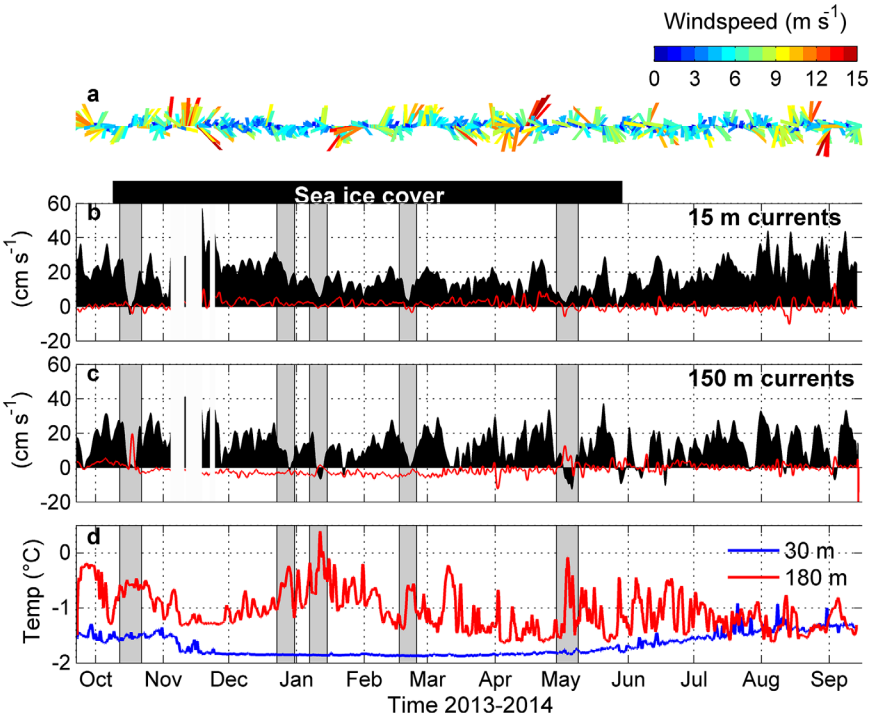

Figure 11. (a) Thirty-six hourly smoothed ERA-I wind speed (m s^{-1}, color) and direction; major (black bars) and minor axis-currents (cm s^{-1}, red line) at (b) 15 m and (c) 150 m; (d) 30 m (blue) and 180 m (red) temperature (°C). Grey bars in middle and bottom panels indicate events where current reversals and coincident temperature increases occur. Black bar over Figure 11b indicates the sea ice cover.

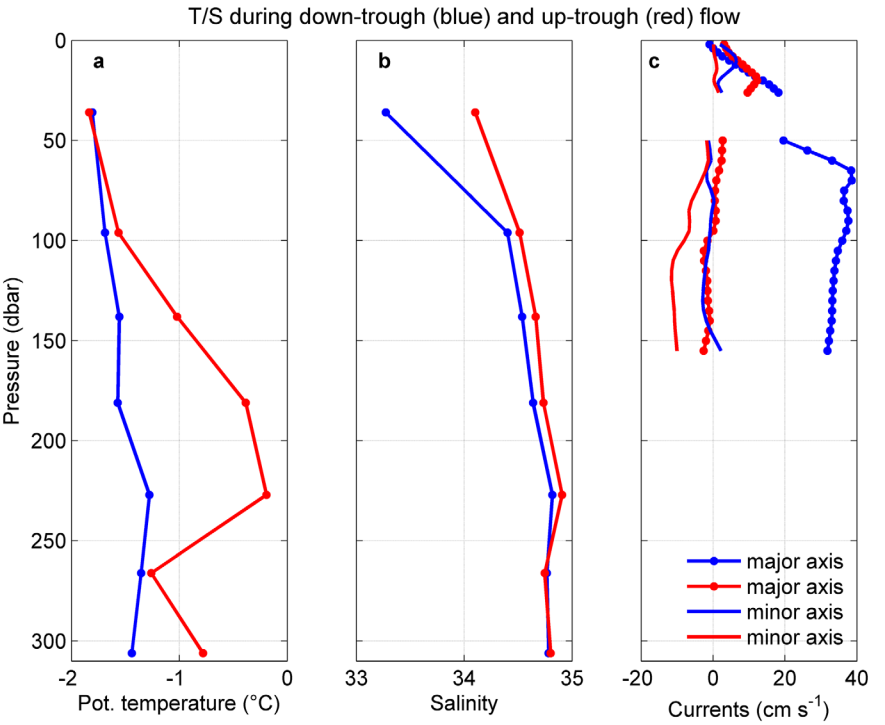

Figure 12. (a) Temperature (°C), (b) salinity, and (c) major-axis-current and minor-axis-current profiles (cm s^{-1}) during "normal" down-trough circulation (blue) and current reversals (red), such as in early May 2014. Dots indicate points of measurements from moored *SBE37* (temperature and salinity) and ADCP bins (currents).

has not yet been captured by the comparatively sparse available data records. Either way, further investigations are needed to better understand relevant exchange processes between the shelf, VT, and the basin, ideally with more than one mooring and complemented by process models as for instance described by *Pickart et al.* [2013].

4.3. Dense Water Formation and Pathways

The UCTD transects from both 2013 and 2014 highlight the presence of cold (<−1.5°C) and saline (>34.5) waters covering depths between 40 and 200 m (Figures 2 and 3). The source of the cold water in 2014 is not clear but was likely carried into the trough with a part of the Barents Sea branch that propagates eastward along the continental slope [*Rudels et al.*, 1994]. The 2013 transect, however, clearly suggests a Laptev Sea shelf source of these cold, saline waters, which indicates that VT can be a pathway for dense waters and potentially relevant to supply Arctic halocline waters [*Aagaard et al.*, 1981]. During the deployment in September 2013, the mooring was located inside the cold water, which changed soon thereafter (Figure 7). Stratification at the mooring was maintained year round, which implies that local dense water formation is insufficient to cause complete convective overturning, but sufficient to produce near-freezing waters with salinities of 34.0–34.5 in the upper 70 m. Besides the near-surface cold dense waters, our mooring showed periods in March–May 2014, when most of the 320 m-deep water column was colder than −1.5°C. The densest waters occurred in late March, when the bottom most 50 m (or more) suddenly cooled to −1.7°C at a maximum salinity of 34.93 (Figure 13). This water mass was still ∼0.2 K above the freezing point at this salinity and thus already modified and not formed locally. Possible formation sites are found throughout the region, as highlighted by recent advances in employing remotely sensed thermal infrared images to detect thin ice and polynya areas [*Willmes and Heinemann*, 2016; *Preußer et al.*, 2016].

Considering the cold and dense water in concert with the vigorous basinward circulation measured at the mooring, it seems plausible that VT is a conduit to supply dense waters to the Nansen Basin. Near-freezing waters were found at a range of salinities, which implies that VT likely impacts a wide depth range of the Arctic Ocean. For instance, the densest waters in VT at 300 m have a higher potential density than waters found at 3000 m depth in the Arctic Ocean, based on a comparison with CTD profiles from the Nansen Basin [*Schauer et al.*, 2012] (Figure 14). Depending on the mixing behavior of dense plumes with surrounding water masses, cold waters observed in VT may supply the Arctic halocline, cool the warm Atlantic layer along the continental slope, and ventilate the deep Arctic Ocean, as was previously discussed by *Rudels et al.* [1994].

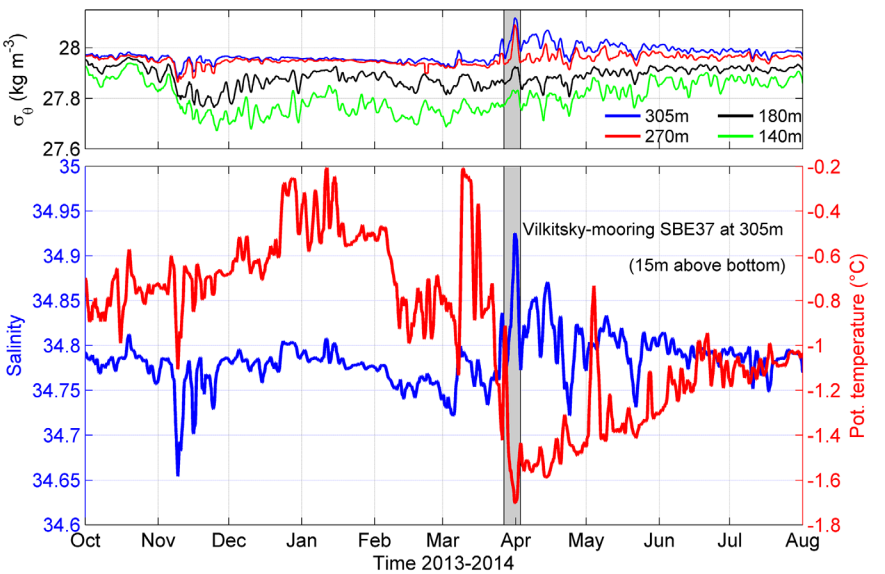

Figure 13. Twenty-four hour low-passed Vilkitsky mooring (a) sigma-ϴ (kg m^{-3}) time series at four depths and the (b) near-bottom (305 m) temperature (°C, red, right *y* axis) and salinity (blue, left *y* axis) record to indicate the water mass evolution during the "dense water" event underlain in grey.

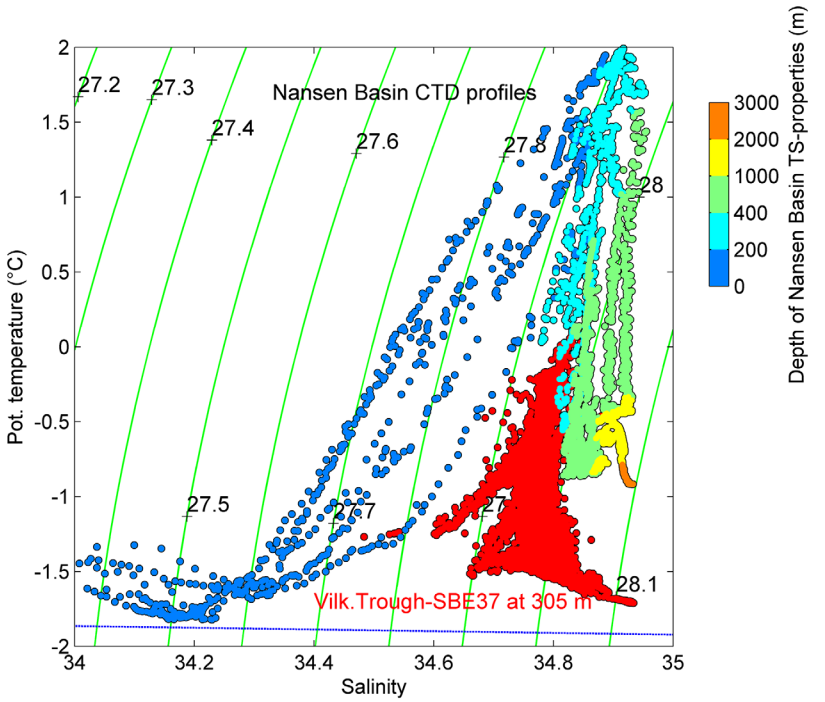

Figure 14. Temperature-salinity diagram relating the potential density from the nearest-to-bottom *SBE37* (red dots) to CTD stations sampled in the Nansen Basin in 2011 [*Schauer et al.*, 2012] (see Figure 1 for locations); the color in T-S from CTD profiles shows the depth of the measurements. Note that the near-bottom sigma-ϴ is >28.0 kg m^{-3} during 13%, and >27.9 kg m^{-3} during 99% of the time within this 1 year deployment.

5. Summary and Conclusion

In this paper, we presented densely spaced UCTD transects from 2013 and 2014 complemented by a 1 year mooring record from Vilkitsky Trough between the Kara and Laptev Seas, an until recently largely

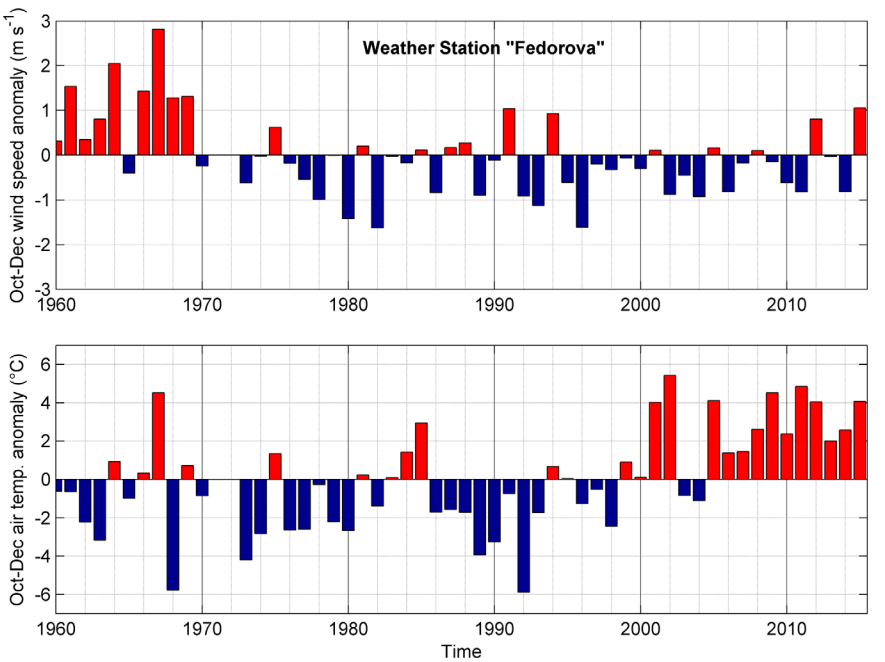

Figure 15. Mean October–December (top) wind speed (m s^{-1}) and (bottom) air temperature (°C) anomalies from 1960 to 2015, measured at a weather station at Cape Chelyuskin in Vilkitsky Strait (see Figure 1 map for location). Note that the positive anomalies after the year 2000 are equally evident when averaged from November to April.

unobserved and poorly understood region in the Eastern Arctic Ocean. The area is a topographically complex crossroads between Siberian River water and the warm Atlantic water boundary current, which loses a considerable amount of heat during its passage between St. Anna Trough and the northern Laptev Sea [*Rudels et al*., 2000; *Pnyushkov et al*., 2015]. The goal of this paper was to provide observational support for recent model results (J15) and to highlight physical processes and parameters that are regionally and Arctic-wide important, and which may suggest further research questions for future model studies and field campaigns. VT is a major pathway for large amounts of freshwater that exit the Kara Sea toward the Arctic Ocean in a surface-intensified current (J15). This was supported by the presence of dilute waters over VT's southern edge in our UCTD transects, associated with considerable thermal wind shear at 20–30 m. A repeat transect near VS showed clear changes in the hydrographic structure following 2 weeks of easterly (upstrait) winds, which implies that short-term variations are relevant in addition to seasonal and interannual variability (J15). Surface and subsurface velocities at the VT-mooring near the mouth of VT are predominantly basinward, which emphasizes a net export of water masses from VT toward the Arctic Ocean.

The deeper (below 100 m) waters in VT were divided by a steep front between Atlantic-derived waters (S $\sim$ 34.85, T $\sim$ 0°C) in the center and near-freezing waters along the edges during both surveys in 2013 and 2014, which implies the presence of dense waters that were likely formed on the adjacent shelves in winter. Both water masses are important Arctic circulation features, and the fate and formation of dense waters and Atlantic water heat sinks are neither understood nor quantified. Individual CTD profiles near the front showed strong temperature interleaving (also indicated in Figure 6), which implies mixing and cooling of the Atlantic-derived waters in the trough and above the continental slope. Atlantic water upwelling, as previously observed in other large Arctic canyons, was not evidenced by our data.

Our VT measurements showed the presence of near-freezing waters at a considerable salinity range in both 2013 and 2014 hydrographic surveys as well as at the mooring at various depth levels, which clearly highlights VT as a conduit for winter-formed dense waters that can impact nearly all layers of the Arctic Ocean. Considering the lack of long-term ocean measurements from this region, it is unclear how this year-long record compares with climatology. A long-term weather station in Vilkitsky Strait showed an abrupt shift in air temperatures after 2000 (Figure 15). Average 2013/2014 winter (November–April) as well as fall (October–December) temperatures were $\sim$2.5°C above the 1960–2015 mean, while wind speed was slightly below average. Winter ice production in Laptev Sea polynyas shows a positive trend especially in fall but was average in 2014 [*Preußer et al*., 2016]. The observed shift toward warmer fall air temperatures implies delays in freezeup. Hence, an overall more dynamic ice cover may explain the positive trends in the region's ice formation and export [*Preußer et al*., 2016], which also favors the production of near-freezing dense waters. Especially topographically channeled wind events such as the November 2013 storm through VS (Figure 10) may amplify down-trough flow and thus inject shelf-transformed and trough-transformed waters into the Nansen Basin. This makes the confluence at the continental slope a potential hotspot for mixing and cross-slope transport, which needs to be thoroughly addressed in future studies.

Acknowledgments
Financial support for the Laptev Sea System project was provided by the German Federal Ministry of Education and Research (grants BMBF 03G0759B/D and 03G0833B/D) and the Ministry of Education and Science of the Russian Federation. The COSMO-CLM model was provided by the German Meteorological Service and the CLM community. Data from the mooring and from the 2013 and 2014 CTD survey can be found at www.Pangaea.de. We greatly acknowledge the Captain and Crew of the *RV Viktor Buinitsky* for safe and successful expeditions, Heidi Kassens as chief scientist and project coordinator, Matthias Monsees for passionate mooring work, Stefan Büttner and Alexey Buinyy for help with the UCTD sampling, and Thomas Krumpen for help with the sea ice drift information. We thank the Editor and two anonymous reviewers for thorough comments and suggestions, which helped to improve the manuscript.

References

Aagaard, K., and E. C. Carmack (1989), The role of sea ice and other fresh water in the Arctic circulation, *J. Geophys. Res.*, *94*(C10), 14,485–14,498, doi:10.1029/JC094iC10p14485.

Aagaard, K., and A. Roach (1990), Arctic Ocean-shelf exchange: Measurements in Barrow Canyon, *J. Geophys. Res.*, *95*(C10), 18,163–18,175.

Aagaard, K., L. K. Coachman, and E. C. Carmack (1981), On the halocline of the Arctic Ocean, *Deep Sea Res., Part A*, *28*, 529–545.

Aksenov, Y., V. V. Ivanov, A. J. G. Nurser, S. Bacon, I. V. Polyakov, A. C. Coward, A. C. Naveira-Garabato, and A. Beszczynska-Moeller (2011), The Arctic Circumpolar Boundary Current, *J. Geophys. Res.*, *116*, C09017, doi:10.1029/2010JC006637.

Bareiss, J., and K. Görgen (2005), Spatial and temporal variability of sea ice in the Laptev Sea: Analyses and review of satellite passive-microwave data and model results, 1979 to 2002, *Global Planet. Change*, *48*(1–3), 28–54.

Batchelor, C. L., and J. A. Dowdeswell (2014), The physiography of High Arctic cross-shelf troughs, *Quat. Sci. Rev.*, *1*(29), 68–96, doi:10.1016/j.quascirev.2013.05.025.

Bauch, D., E. Cherniavskaia, and L. Timokhov (2016), Shelf basin exchange along the Siberian continental margin: Modification of Atlantic Water and Lower Halocline Water, *Deep Sea Res., Part I*, *115*, 188–198, doi:10.1016/j.dsr.2016.06.008.

Bauer, M., D. Schröder, G. Heinemann, S. Willmes, and L. Ebner (2013), Quantifying polynya ice production in the Laptev Sea with the COSMO model, *Polar Res.*, *32*, 20922, doi:10.3402/polar.v32i0.20922.

Belliveau, D. J., G. L. Bugden, B. M. Eid, and C. J. Cainan (1990), Sea ice velocity measurements by upward-looking Doppler current profilers, *J. Atmos. Oceanic Technol.*, *7*, 596–602.

Berezkin, V. A., and G. Y. Ratmanov (1940), A general scheme of currents of the Arctic Ocean and adjacent seas, in *Hydrograpic Administration of the Navy* [in Russian], 10 pp., Leningrad.

Carmack, E., F. McLaughlin, M. Yamamoto-Kawai, M. Itoh, K. Shimada, R. Krishfield, and A. Proshutinsky (2008), Freshwater storage in the Northern Ocean and the special role of the Beaufort Gyre, in *Arctic-Subarctic Ocean Fluxes: Defining the Role of the Northern Seas in Climate*, edited by R. R. Dickson, J. Meincke, and P. Rhines, pp. 145–170, Springer, Dordrecht, Netherlands.

Coachman, L. K., and C. A. Barnes (1962), Surface water in the Eurasian Basin of the Arctic Ocean, *Arctic*, *15*(4), 251–277.

Dai, A., and K. E. Trenberth (2002), Estimates of freshwater discharge from continents: Latitudinal and seasonal variations, *J. Hydrometeorol.*, *3*, 660–687.

Dee, D. P., et al. (2011), The ERA-Interim reanalysis: Configuration and performance of the data assimilation system, *Q. J. R. Meteorol. Soc.*, *137*, 553–597, doi:10.1002/qj.828.

Divine, D. V., R. Korsnes, and A. P. Makshtas (2004), Temporal and spatial variation of shore-fast ice in the Kara Sea, *Cont. Shelf Res.*, *24*, 1717–1736, doi:10.1016/j.csr.2004.05.010.

Dmitrenko, I. A., S. A. Kirillov, L. B. Tremblay, D. Bauch, J. A. Hölemann, T. Krumpen, H. Kassens, C. Wegner, G. Heinemann, and D. Schröder (2010), Impact of the Arctic Ocean Atlantic water layer on Siberian shelf hydrography, *J. Geophys. Res.*, *115*, C08010, doi:10.1029/2009JC006020.

Dmitrenko, I. A., et al. (2014), Heat loss from the Atlantic water layer in the northern Kara Sea: Causes and consequences, *Ocean Sci.*, *10*, 719–730, doi:10.5194/os-10-719-2014.

Girard-Ardhuin, F., and R. Ezraty (2012), Enhanced Arctic sea ice drift estimation merging radiometer and scatterometer data, *IEEE Trans. Geosci. Remote Sens.*, *50*, 2639–2648, doi:10.1109/TGRS.2012.2184124.

Grebmeier, J. M., et al. (2015), Ecosystem characteristics and processes facilitating persistent macrobenthic biomass hotspots and associated benthivory in the Pacific Arctic, *Prog. Oceanogr.*, *136*, 92–114.

Gutjahr, O., G. Heinemann, A. Preußer, S. Willmes, and C. Drüe (2016), Quantification of ice production in Laptev Sea polynyas and its sensitivity to thin-ice parameterizations in a regional climate model, *Cryosphere*, *10*, 2999–3019, doi:10.5194/tc-2016-83.

Hanzlick, D., and K. Aagaard (1980), Freshwater and Atlantic Water in the Kara Sea, *J. Geophys. Res.*, *85*(C9), 4937–4942.

Harms, I. H., and M. J. Karcher (1999), Modeling the seasonal variability of hydrography and circulation in the Kara Sea, *J. Geophys. Res.*, *104*(C6), 13,431–13,448.

Harms, I. H., and M. J. Karcher (2005), Kara Sea freshwater dispersion and export in the late 1990s, *J. Geophys. Res.*, *110*, C08007, doi:10.1029/2004JC002744.

Itoh, M., R. S. Pickart, T. Kikuchi, Y. Fukamachi, K. I. Ohshima, D. Simizu, K. R. Arrigo, S. Vagle, J. He, and C. Ashjian (2015), Water properties, heat and volume fluxes of Pacific water in Barrow Canyon during summer 2010, *Deep Sea Res., Part I*, *102*, 43–54.

Ivanov, V. V., and P. N. Golovin (2007), Observations and modeling of dense water cascading from the northwestern Laptev Sea shelf, *J. Geophys. Res.*, *112*, C09003, doi:10.1029/2006JC003882.

Jakobsson, M., R. Macnab, L. Mayer, R. Anderson, M. Edwards, J. Hatzky, H. W. Schenke, and P. Johnson (2008), An improved bathymetric portrayal of the Arctic Ocean: Implications for ocean modeling and geological, geophysical and oceanographic analyses, *Geophys. Res. Lett.*, *35*, L07602, doi:10.1029/2008GL033520.

Janout, M. A., and Y. D. Lenn (2014), Semidiurnal tides on the Laptev Sea shelf based on oceanographic moorings with implications for shear and vertical mixing, *J. Phys. Oceanogr.*, *44*(1), 202–219, doi:10.1175/JPO-D-12-0240.1.

Janout, M. A., J. Hölemann, and T. Krumpen (2013), Cross-shelf transport of warm and saline water in response to sea ice drift on the Laptev Sea shelf, *J. Geophys. Res. Oceans*, *118*, 563–576, doi:10.1029/2011JC007731.

Janout, M. A., et al. (2015), Kara Sea freshwater transport through Vilkitsky Strait: Variability, forcing, and further pathways toward the western Arctic Ocean from a model and observations, *J. Geophys. Res. Oceans*, *120*, 4925–4944, doi:10.1002/2014JC010635.

Kaiser, K., R. Benner, and R. M. W. Amon (2017), The fate of terrigenous dissolved organic carbon on the Eurasian shelves and export to the North Atlantic, *J. Geophys. Res. Oceans*, *122*, 4–22, doi:10.1002/2016JC012380.

Kalnay, E., et al. (1996), The NCEP/NCAR 40-year reanalysis project, *Bull. Amer. Meteorol. Soc.*, *77*, 437–471.

Krumpen, T., M. A. Janout, K. I. Hodges, R. Gerdes, F. Ardhuin, J. A. Hoelemann, and S. Willmes (2013), Variability and trends in Laptev Sea ice outflow between 1992–2011, *The Cryosphere*, *7*(1), 349–363.

Martin, S., and D. J. Cavalieri (1989), Contributions of the Siberian shelf polynyas to the Arctic Ocean intermediate and deep water, *J. Geophys. Res.*, *94*(C9), 12,725–12,738, doi:10.1029/JC094iC09p12725.

Moore, G. W. K. (2013), The Novaya Zemlya Bora and its impact on Barents Sea air-sea interaction, *Geophys. Res. Lett.*, *40*, 3462–3467, doi:10.1002/grl.50641.

Moore, G. W. K., I. A. Renfrew, B. E. Harden, and S. H. Mernild (2015), The impact of resolution on the representation of southeast Greenland barrier winds and katabatic flows, *Geophys. Res. Lett.*, *42*, 3011–3018, doi:10.1002/2015GL063550.

Morison, J., R. Kwok, C. Peralta-Ferriz, M. Alkire, I. Rigor, R. Andersen, and M. Steele (2012), Changing Arctic Ocean freshwater pathways, *Nature*, *481*, 66–70, doi:10.1038/nature10705.

Mountain, D. G., L. K. Coachman, and K. Aagaard (1976), On the flow through Barrow Canyon, *J. Phys. Oceanogr.*, *6*, 461–470.

Panteleev, G., A. Proshutinsky, M. Kulakov, D. A. Nechaev, and W. Maslowski (2007), Investigation of the summer Kara Sea circulation employing a variational data assimilation technique, *J. Geophys. Res.*, *112*, C04S15, doi:10.1029/2006JC003728.

Pavlov, V. K., L. A. Timokhov, G. A. Baskakov, M. Y. Kulakov, V. K. Kurazhov, P. V. Pavlov, S. V. Pivovoarov, and V. V. Stanovoy (1996), Hydrometeorological regime of the Kara, Laptev, and East-Siberian Seas, *Tech. Memo. APL-UW TM* 1–96, 179 pp., Appl. Phys. Lab., Univ. of Wash., Seattle.

Pawlowicz, R., B. Beardsley, and S. Lentz (2002), Classical tidal harmonic analysis including error estimates in MATLAB using T_TIDE, *Comput. Geosci.*, *28*, 929–937.

Perovich, D. K., J. A. Richter-Menge, K. F. Jones, and B. Light (2008), Sunlight, water, and ice: Extreme Arctic sea ice melt during the summer of 2007, *Geophys. Res. Lett.*, *35*, L11501, doi:10.1029/2008GL034007.

Pickart, R. S., G. W. K. Moore, D. J. Torres, P. S. Fratantoni, R. A. Goldsmith, and J. Yang (2009), Upwelling on the continental slope of the Alaskan Beaufort Sea: Storms, ice, and oceanographic response, *J. Geophys. Res.*, *114*, C00A13, doi:10.1029/2008JC005009.

Pickart, R. S., M. A. Spall, and J. T. Mathis (2013), Dynamics of upwelling in the Alaskan Beaufort Sea and associated shelf–basin fluxes, *Deep Sea Res., Part I*, *176*, 35–51.

Pnyushkov, A. V., I. V. Polyakov, V. V. Ivanov, Y. Aksenov, A. C. Coward, M. Janout, and B. Rabe (2015), Structure and variability of the boundary current in the Eurasian Basin of the Arctic Ocean, *Deep Sea Res., Part I*, *101*, 80–97, doi:10.1016/j.dsr.2015.03.001.

Preußer, A., G. Heinemann, S. Willmes, and S. Paul (2016), Circumpolar polynya regions and ice production in the Arctic: Results from MODIS thermal infrared imagery for 2002/2003 to 2014/2015 with a regional focus on the Laptev Sea, *Cryosphere*, *10*, 3021–3042, doi:10.5194/tc-2016-133.

Proshutinsky, A., R. Krishfield, M.-L. Timmermans, J. Toole, E. Carmack, F. McLaughlin, W. J. Williams, S. Zimmermann, M. Itoh, and K. Shimada (2009), Beaufort Gyre freshwater reservoir: State and variability from observations, *J. Geophys. Res.*, *114*, C00A10, doi:10.1029/2008JC005104.

Proshutinksy, A. Y., and M. A. Johnson (1997), Two circulation regimes of the wind-driven Arctic Ocean, *J. Geophys. Res.*, *102*, 12,493–12,514.

Rabe, B., M. Karcher, F. Kauker, U. Schauer, J. M. Toole, R. A. Krishfield, S. Pisarev, T. Kikuchi, and J. Su (2014), Arctic Ocean basin liquid freshwater storage trend 1992–2012, *Geophys. Res. Lett.*, *41*, 961–968, doi:10.1002/2013GL058121.

Rockel, B., A. Will, and A. Hense (2008), The Regional Climate Model COSMO-CLM (CCLM), *Meteorol. Z.*, *17*(4), 347–348, doi: 10.1127/0941-2948/2008/0309.

Rudels, B., E. P. Jones, L. G. Anderson, and G. Kattner (1994), On the intermediate depth waters of the Arctic Ocean, in *The Polar Oceans and Their Role in Shaping the Global Environment: The Nansen Centennial Volume, Geophys. Monogr. Ser.*, vol. 84985, edited by O. M. Johannessen, R. D. Muench, and J. E. Overland, pp. 33–46, AGU, Washington, D. C.

Rudels, B., R. D. Muench, J. Gunn, U. Schauer, and H. J. Friedrich (2000), Evolution of the Arctic Ocean boundary current north of the Siberian shelves, *J. Mar. Syst.*, *25*, 77–99.

Schauer, U., R. D. Muench, B. Rudels, and L. Timokhov (1997), Impact of eastern Arctic shelf waters on the Nansen Basin intermediate layers, *J. Geophys. Res.*, *102*(C2), 3371–3382.

Schauer, U., B. Rabe, and A. Wisotzki (2012), *Physical oceanography during POLARSTERN cruise ARK-XXVI/3 (TransArc)*, Alfred Wegener Inst., Helmholtz Cent. for Polar and Mar. Res., Bremerhaven, Germany, doi:10.1594/PANGAEA.774181.

Serreze, M. C., A. P. Barrett, A. G. Slater, R. A. Woodgate, K. Aagaard, R. B. Lammers, M. Steele, R. Moritz, M. Meredith, and C. M. Lee (2006), The large-scale freshwater cycle of the Arctic, *J. Geophys. Res.*, *111*, C11010, doi:10.1029/2005JC003424.

Spall, M. A. (2013), On the circulation of Atlantic Water in the Arctic Ocean, *J. Phys. Oceanogr.*, *43*, 2352–2371, doi:10.1175/JPO-D-13-079.1.

Timokhov, L. A., J. Hölemann, A. Y. Ipatov, M. A. Janout, and H. Kassens (2015), Cold shelf waters of the Laptev Sea in the summer of 2013, *Probl. Arctic Antarct.*, *2*(104), 81–92.

Volkov, V. A., O. M. Johannessen, V. E. Boradachev, G. N. Voinov, L. H. Pettersson, L. P. Bobylev, and A. V. Kouraev (2002), *Polar Seas Oceanography: An Integrated Case Study of the Kara Sea*, Springer, New York.

Weingartner, T. J., D. J. Cavalieri, K. Aagaard, and Y. Sasaki (1998), Circulation, dense water formation, and outflow on the Northeast Chukchi shelf, *J. Geophys. Res.*, *103*(C4), 7647–7661.

Wentz, F., T. Meissner, C. Gentemann, K. Hilburn, and J. Scott (2014), *Remote Sensing Systems GCOM-W1 AMSR2 Daily Environmental Suite on 0.25 deg Grid, Version 7.2*, Remote Sens. Syst., Santa Rosa, Calif. [Available at www.rems.com/missions/amsre.]

Williams, W. J., E. C. Carmack, K. Shimada, H. Melling, K. Aagaard, R. W. Macdonald, and R. G. Ingram (2006), Joint effects of wind and ice motion in forcing upwelling in Mackenzie Trough, Beaufort Sea, *Cont. Shelf Res.*, *26*, 2351–2366.

Willmes, S., and G. Heinemann (2016), Sea-ice wintertime lead frequencies and regional characteristics in the Arctic, 2003–2015, *Remote Sens.*, *8*, 4.

Zhang, J., and D. A. Rothrock (2003), Modeling Global Sea Ice with a thickness and enthalpy distribution model in generalized curvilinear coordinates, *Mon. Weather Rev.*, *131*(5), 845–861, doi:10.1175/1520-0493/2003)131 < 0845:MGSIWA>2.0.CO;2.

Zhang, J., and M. Steele (2007), Effect of vertical mixing on the Atlantic Water layer circulation in the Arctic Ocean, *J. Geophys. Res.*, *112*, C04S04, doi:10.1029/2006JC003732.